IEEE Photonics Journal
An IEEE Photonics Society Publication

Open Access

Analysis of a Silicon Reconfigurable Feed-Forward Optical Delay Line

Volume 6, Number 1, February 2014

Zhilong Chen
Linjie Zhou, Member, IEEE
Jianping Chen

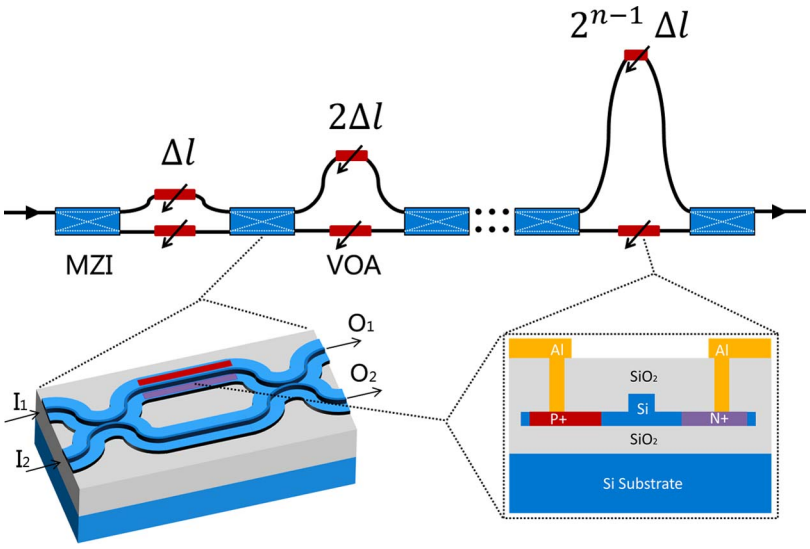

DOI: 10.1109/JPHOT.2013.2292697
1943-0655

IEEE photonics SOCIETY

IEEE

Analysis of a Silicon Reconfigurable Feed-Forward Optical Delay Line

Zhilong Chen, Linjie Zhou, *Member, IEEE*, and Jianping Chen

State Key Laboratory of Advanced Optical Communication Systems and Networks, Department of Electronic Engineering, Shanghai Jiao Tong University, Shanghai 200240, China

DOI: 10.1109/JPHOT.2013.2292697

Manuscript received October 21, 2013; revised November 20, 2013; accepted November 20, 2013. Date of publication November 25, 2013; date of current version January 3, 2014. This work was supported in part by the 973 Program under Grant ID2011CB301700; by the 863 Program under Grant 2013AA014402; by the National Natural Science Foundation of China (NSFC) under Grants 61007039, 61001074, and 61127016; by the Science and Technology Commission of Shanghai Municipality (STCSM) under Project 12XD1406400; and by the State Key Laboratory Project under Grant GKZD030024. Corresponding author: L. Zhou (e-mail: ljzhou@sjtu.edu.cn).

Abstract: We analyze a silicon reconfigurable feed-forward optical delay line (ODL) composed of cascaded Mach–Zehnder interferometer (MZI) switches and waveguide delay pairs. Optical delay is step-tuned by switching among optical routes with an incremental length difference. The crosstalk caused by limited extinction ratios (ERs) of MZI switches and the waveguide loss restricts the ODL buffering capacity. A method to suppress the crosstalk and hence expand the buffering capacity is proposed by inserting variable optical attenuators (VOAs) between successive MZI switches. A design example shows that a seven-stage ODL without VOAs can delay 8–98 bits with a tuning step of 1 bit for a 40 Gbit/s non-return-to-zero (NRZ) $2^{13} - 1$ pseudo-random bit sequence (PRBS) optical signal. When VOAs with a 10 dB attenuation ratio are included, the signal-to-crosstalk ratio (SCR) of the output signal is increased by 17 dB on average, making the ODL capable of delaying 8–135 bits at its maximum.

Index Terms: Optical delay line (ODL), Mach–Zehnder interferometer (MZI), variable optical attenuator (VOA), silicon photonics, integrated optical device.

1. Introduction

Optical buffers are widely investigated in the last decade because of their potential applications in all-optical communication systems [1]–[4]. With the development of silicon photonics, as one of the most promising optical platforms for future optical communications and interconnects, it is feasible to implement on-chip silicon optical buffers and integrate them into photonic integrated circuits (PIC) [5]–[8]. Several approaches have been proposed to realize chip-scale optical buffering devices [9]. Coupled resonator structures (CRS) and optical delay lines (ODL) are the two most popular methods. In the CRS-based optical buffers, microrings [10]–[12] or photonic crystals [13]–[15] are used to delay optical signals. By changing the refractive index of the resonators, a continuously tunable optical buffer can be realized. For ODL-based optical buffers, optical signals are switched among waveguides with different lengths to make a discretely tunable delay [16]–[18]. Since the CRS has large group delay dispersion (GDD) around resonance, the optical signal inevitably suffers dispersion while being delayed [19]–[21]. ODL outperforms CRS in terms of the quality of transmitted signal but at the expense of a larger footprint [1], [9].

Reconfigurable feed-forward delay lines are one of the basic ODL structures as shown in Fig. 1(a). Because of their straight-forward configuration and easy control, they can be readily applied in

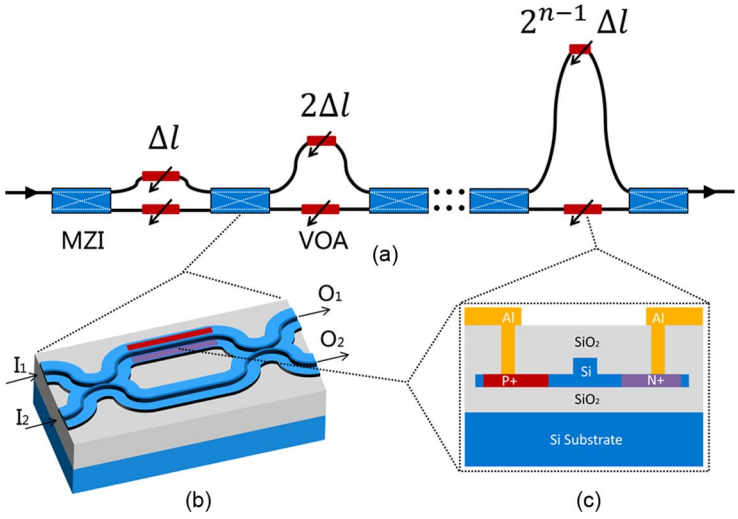

Fig. 1. (a) Schematic illustration of the silicon reconfigurable feed-forward optical delay line. (b) 3-D view of the single-armed-modulated Mach–Zehnder interferometer used as an optical switch. (c) Cross-sectional view of the p-i-n diode for optical phase tuning (in MZI switch) and optical power attenuation (in VOA).

telecommunications and all-optical signal processing. Since optical switches, for example, Mach–Zehnder interferometer (MZI)-based switches in Fig. 1(b), are not perfect in practice, they cannot have infinite extinction ratio (ER) for the two output ports, which causes the residual signal to interfere with the major one, resulting in inter-symbol crosstalk and thus degrading signal-to-crosstalk ratio (SCR).

In this paper, we present a silicon reconfigurable feed-forward ODL which employs MZI switches and waveguide delay pairs to realize a step-type tunable optical buffer. We investigate the two main factors that degrade the quality of the output optical signal including the crosstalk resulted from the limited ER of switches and the waveguide propagation loss. We use a 40 Gbit/s non-return-to-zero (NRZ) $2^{13}-1$ pseudo-random bit sequence (PRBS) data at 1550 nm wavelength to characterize its transmission performances. SCR and eye diagram are examined for all possible delay combinations. Finally, a method to improve the buffering capacity of the ODL by inserting variable optical attenuators (VOA) to suppress the crosstalk is proposed and analyzed.

2. Device Structure and Modeling

2.1. Working Principle

Fig. 1 shows the schematic of the proposed step-tuning silicon reconfigurable feed-forward ODL. The device consists of $N+1$ cascaded 2×2 MZI switches with p-i-n diodes integrated in one arm for phase tuning. One pair of waveguides with different lengths connects two successive MZIs. The length difference of the waveguides in the next stage is twice the length difference in the previous stage. Upon selecting different routes by control of the MZIs, the signal can experience various time delays. Note that VOAs can be inserted into each waveguide as depicted in Fig. 1(a) to attenuate the residual signal in order to improve the quality of the transmitted signal, as will be discussed later.

The transmission of light wave though the ODL can be modeled by the transfer matrix method. The transfer matrix of an N-stage ODL (namely $N+1$ MZIs) is expressed as

$$T=\begin{pmatrix} T_{11}(\omega) & T_{12}(\omega) \\ T_{21}(\omega) & T_{22}(\omega) \end{pmatrix} = M_{N+1}\left(\prod_{k=1}^{N} D_k M_k\right) \tag{1}$$

where M_k and D_k represent the transfer matrices of the kth MZI switch and the kth waveguide pair.

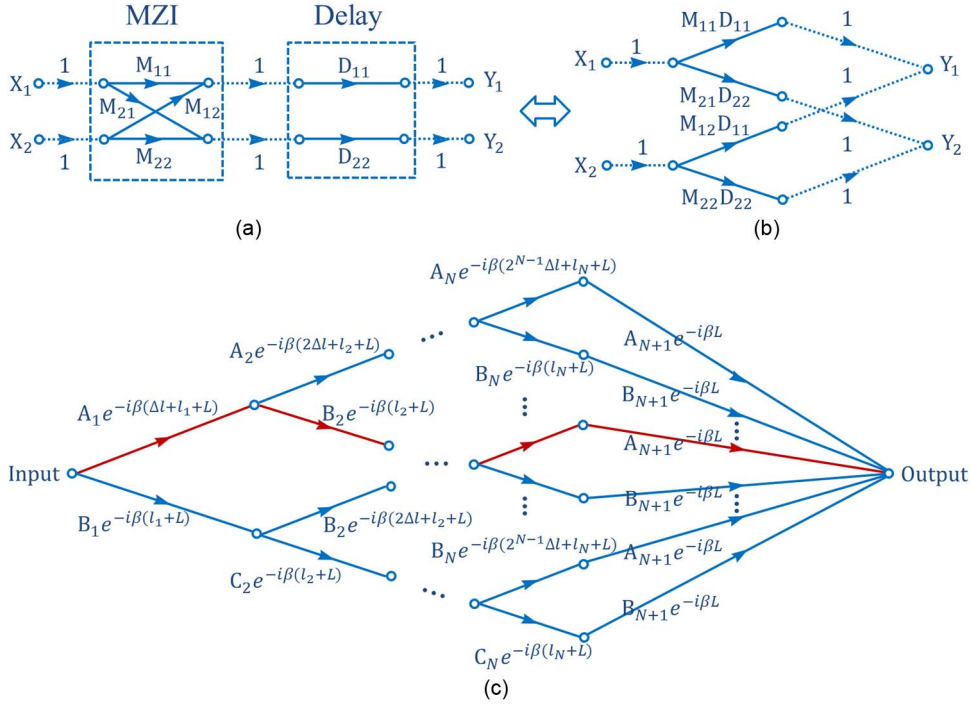

Fig. 2. (a) Signal-flow graph for a delay unit (one MZI switch and one waveguide pair). (b) Equivalent transformation of (a). (c) Signal-flow graph of the entire ODL. The red line represents the main signal path.

The transfer matrix of the MZI switch is given by

$$M_k = \begin{pmatrix} M_{11}^{(k)} & M_{12}^{(k)} \\ M_{21}^{(k)} & M_{22}^{(k)} \end{pmatrix} = \begin{pmatrix} \tau & -\mathrm{i}\kappa \\ -\mathrm{i}\kappa & \tau \end{pmatrix} \begin{pmatrix} \mathrm{e}^{-\mathrm{i}\left(\beta+\Delta\beta^{(\mathrm{m})}\right)L} & 0 \\ 0 & e^{-\mathrm{i}\beta L} \end{pmatrix} \begin{pmatrix} \tau & -\mathrm{i}\kappa \\ -\mathrm{i}\kappa & \tau \end{pmatrix}$$
$$= \begin{pmatrix} \left(\tau^2 e^{-\mathrm{i}\Delta\beta^{(\mathrm{m})}L} - \kappa^2\right)\mathrm{e}^{-\mathrm{i}\beta L} & -\mathrm{i}\tau\kappa\left(\mathrm{e}^{-\mathrm{i}\Delta\beta^{(\mathrm{m})}L} + 1\right)\mathrm{e}^{-\mathrm{i}\beta L} \\ -\mathrm{i}\tau\kappa\left(e^{-\mathrm{i}\Delta\beta^{(\mathrm{m})}L} + 1\right)\mathrm{e}^{-\mathrm{i}\beta L} & \left(-\kappa^2\mathrm{e}^{-\mathrm{i}\Delta\beta^{(\mathrm{m})}L} + \tau^2\right)\mathrm{e}^{-\mathrm{i}\beta L} \end{pmatrix} = \mathrm{e}^{-\mathrm{i}\beta L}\begin{pmatrix} A_k & B_k \\ B_k & C_k \end{pmatrix} \quad (2)$$

where τ and κ are the transmission coefficient and the coupling coefficient of the coupler, respectively ($\tau^2 + \kappa^2 = 1$ for lossless coupling), L is the length of the two arms, β is the propagation constant of the arm waveguide, $\Delta\beta$ represents the change of β on the active arm and the superscript (m) denotes whether the p-i-n diode is tuned on or off. Note that the magnitudes of A_k, B_k and C_k are equal to 0 or 1 for ideal MZI switches. The transfer matrix D_k is given by

$$D_k = \begin{pmatrix} D_{11}^{(k)} & D_{12}^{(k)} \\ D_{21}^{(k)} & D_{22}^{(k)} \end{pmatrix} = \begin{pmatrix} \mathrm{e}^{-\mathrm{i}\beta\left(2^{k-1}\Delta l + l_k\right)} & 0 \\ 0 & \mathrm{e}^{-\mathrm{i}\beta l_k} \end{pmatrix} \quad (3)$$

where $2^{k-1}\Delta l + l_k$ and l_k are the lengths of the long waveguide and short waveguide on the kth stage, respectively.

$T_{11}(\omega)$ is the transfer function of the ODL, assuming the input port is I_1 of the 1st MZI [denoted in Fig. 1(b)] and the output port is O_1 of the $(N+1)$th MZI. In our following analysis, we will use the signal-flow graph (SFG) to simplify the expression for $T_{11}(\omega)$ so that its physical meaning is more straight-forward.

Fig. 2(a) is the equivalent SFG for $D_k \cdot M_k$ (the dashed lines weighted 1 are only auxiliary routes to make the signal flow clear). We can transform Fig. 2(a) equivalently into Fig. 2(b). In such a way, the SFG for the entire device can be drawn as Fig. 2(c). Note that Fig. 2(c) has a similar structure to

a binary tree, and has 2^N routes from the input to the output. In practice, the MZI cannot have an infinite ER for the two output ports. When the split light does not perfectly interfere in the MZI, parts of the energy will be lost from the main path and coupled into the other path. In our cascaded feed-forward ODL, the lost energy will be coupled back and interfere with the main one in the next MZI switch, resulting in crosstalk. The crosstalk accumulates in the following MZIs and eventually deteriorates the signal. Assume that the red line in Fig. 2(c) is the main route that the signal passes and then the remained $2^N - 1$ routes are the branches that generate crosstalk. Therefore, $T_{11}(\omega)$ can be expressed as

$$T_{11}(\omega) = \sum_{n=0}^{2^N-1} S_n \mathrm{e}^{-\mathrm{i}\beta\left[n\Delta l + \sum_{k=1}^{N} l_k + (N+1)L\right]} \tag{4}$$

where S_n is the product of A_k, B_k, and C_k $(k = 1, 2, \ldots N+1)$, as derived from Fig. 2(c).

When the residual signal on each branch route is low compared to the main one, the group delay of the ODL can be derived as

$$t_{\mathrm{g}} = -\frac{\partial \prec T_{11}(\omega)}{\partial \omega} \cong \left[\left(\sum_{k=1}^{N} a_k 2^{k-1}\right)\Delta l + \sum_{k=1}^{N} l_k + (N+1)L\right] \cdot \frac{\partial \mathrm{Re}(\beta)}{\partial \omega} \tag{5}$$

where a_k is the configuration parameter of the ODL. $a_k = 1$ if the signal propagates through the long waveguide in the kth stage, and $a_k = 0$ if it is through the short waveguide. As a result, the switching states of MZIs are determined by a_k. If $a_k = a_{k-1}$, the kth MZI is in the "bar" state, otherwise in the "cross" state. The assumption of low residual signal in Eq. (5) is necessary, since the group delay of ODL will become meaningless if the signal is submerged in the crosstalk.

Therefore, we can deduce from Eq. (5) that the delay range of the ODL is

$$t_{\max} = \frac{n_{\mathrm{g}}\left((2^N - 1)\Delta l + \sum_{k=1}^{N} l_k + (N+1)L\right)}{c} \tag{6}$$

$$t_{\min} = \frac{n_{\mathrm{g}}\left(\sum_{k=1}^{N} l_k + (N+1)L\right)}{c} \tag{7}$$

and the ODL is discretely tunable with a delay step equal to

$$\Delta t = \frac{n_{\mathrm{g}}\Delta l}{c} \tag{8}$$

where n_{g} are the group refractive index of the waveguide.

2.2. MZI Switch

To analyze the SCR of the output signal, it is necessary to investigate the cause of the crosstalk, i.e., the limited ER of MZI. The limited ER of a 2×2 MZI origins from the imbalance of optical power in the two arms, uneven splitting ratio of the couplers, and the phase errors in the two arms. The power imbalance may come from the unequal propagation loss between the two arms. For silicon MZI switches using free-carrier plasma dispersion (FCD) effect, there is an inherent power imbalance fact because the free-carrier absorption (FCA) always accompanies the refractive index change. We will firstly analyze the influence of phase tuning on ERs of MZI and then take other factors into account.

To utilize the FCD effect, p-i-n diodes are embedded in one of the MZI arms for electrical phase tuning. Such a p-i-n diode based phase shifter has been widely demonstrated as a reliable and promising component in a variety of devices and chips [22]–[24]. Fig. 1(b) shows the 3-D perspective view of the tunable MZI switch unit. It consists of two balanced arms and two 2×2 3-dB

couplers in the input and output ends. With the FCA loss taken into consideration, the ERs of the output ports of a single-arm-modulated MZI are derived from Eq. (2) as (input from I_1)

$$\mathrm{ER}_1 = 10\log_{10}\left|\frac{M_{11}^{\mathrm{bar}}}{M_{11}^{\mathrm{cross}}}\right|^2 = 20\log_{10}\left(\frac{1+e^{\mathrm{Im}(\Delta\beta^{\mathrm{m}})L}}{1-e^{\mathrm{Im}(\Delta\beta)L}}\right) \tag{9}$$

$$\mathrm{ER}_2 = 10\log_{10}\left|\frac{M_{21}^{\mathrm{cross}}}{M_{21}^{\mathrm{bar}}}\right|^2 = 20\log_{10}\left(\frac{1+e^{\mathrm{Im}(\Delta\beta L)}}{1-e^{\mathrm{Im}(\Delta\beta^{\mathrm{m}}L)}}\right). \tag{10}$$

Here, L is the arm length which assures $\mathrm{Re}(\Delta\beta^{\mathrm{m}})L$ equal to π. $\Delta\beta^{\mathrm{m}}$ is a carrier-concentration dependent perturbation of the propagation constant β, which is given by

$$\Delta\beta^{\mathrm{m}} = \frac{2\pi}{\lambda}\left(\Delta n_{\mathrm{eff}} - \mathrm{i}\frac{\lambda}{4\pi}\Delta\alpha_{\mathrm{eff}}\right) \tag{11}$$

$\mathrm{Re}(\Delta\beta^{\mathrm{m}})$ and $\mathrm{Im}(\Delta\beta^{\mathrm{m}})$ are related to the change of refractive index (Δn) and absorption coefficient $(\Delta\alpha)$, respectively.

Fig. 1(c) is the cross-sectional view of the phase shifter. Under a forward-bias, free carriers are injected into the waveguide region, inducing changes in both Δn and $\Delta\alpha$. Useful empirical expressions for Δn and $\Delta\alpha$ in silicon at 1550 nm were quantified by Soref and Bennett as [25]

$$\Delta n = -\left[8.8\times10^{-22}\cdot\Delta N_{\mathrm{e}} + 8.5\times10^{-18}\cdot(\Delta N_{\mathrm{h}})^{0.8}\right] \tag{12}$$

$$\Delta\alpha = 8.5\times10^{-18}\cdot\Delta N_{\mathrm{e}} + 6.0\times10^{-18}\cdot\Delta N_{\mathrm{h}} \tag{13}$$

where ΔN_{e} and ΔN_{h} are the change of electron and hole densities in the waveguide, respectively.

The effective refractive index change and the effective absorption coefficient change are calculated through the overlap integral with the optical mode as [26]

$$\Delta n_{\mathrm{eff}} = \frac{\iint \Delta n(x,y)|E(x,y)|^2 dxdy}{\iint |E(x,y)|^2 dxdy} \tag{14}$$

$$\Delta\alpha_{\mathrm{eff}} = \frac{\iint \Delta\alpha(x,y)|E(x,y)|^2 dxdy}{\iint |E(x,y)|^2 dxdy} \tag{15}$$

where $E(x,y)$ is the mode electric field cross-sectional distribution.

We employ a 2D simulation package ATLAS from SILVACO to calculate the carrier distribution in the p-i-n diode under a forward-bias. The waveguide width is 500 nm and the height is 220 nm with a 60 nm slab left to form lateral p-i-n diode. Both the heavily doped p+ and the n+ regions have a doping concentration of 10^{20} cm^{-3} for ohmic contact. Both the doping regions are separated by 500 nm from the waveguide sidewall to ensure low FCA loss.

Fig. 3(a) depicts the simulation results of the cross-sectional electron distribution under 0 V, 0.5 V, and 0.8 V. Fig. 3(b) illustrates the effective refractive index and absorption coefficient change as a function of forward-bias voltage. Both Δn_{eff} (absolute value) and $\Delta\alpha_{\mathrm{eff}}$ increase rapidly once the p-i-n diode is tuned on after $\sim$0.7 V, which implies a tradeoff between the phase shift and the absorption loss. Fig. 3(c) shows the ERs at the two output ports resulted from the FCA. The arm length is varied from 200 μm to 3.7 mm, which corresponds to a π-phase shift voltage V_π from 0.95 V to 0.76 V. Note that ER_2 is much smaller than ER_1 because the optical power cannot be totally switched off after π-phase shift due to the FCA.

With additional factors including uneven splitting ratio of the couplers and phase errors in the arms taken into consideration, the ERs can be modified as

$$\mathrm{ER}_1 = 10\log_{10}\left[\frac{1+\left(\frac{\tau^2}{\kappa^2}e^{-\Delta\alpha_{\mathrm{eff}}^{\mathrm{m}}L/2}\right)^2 + 2\frac{\tau^2}{\kappa^2}e^{-\Delta\alpha_{\mathrm{eff}}^{\mathrm{m}}L/2}\cos\theta}{1+\left(\frac{\tau^2}{\kappa^2}e^{-\Delta\alpha_{\mathrm{eff}}L/2}\right)^2 - 2\frac{\tau^2}{\kappa^2}e^{-\Delta\alpha_{\mathrm{eff}}L/2}\cos\theta}\right] \tag{16}$$

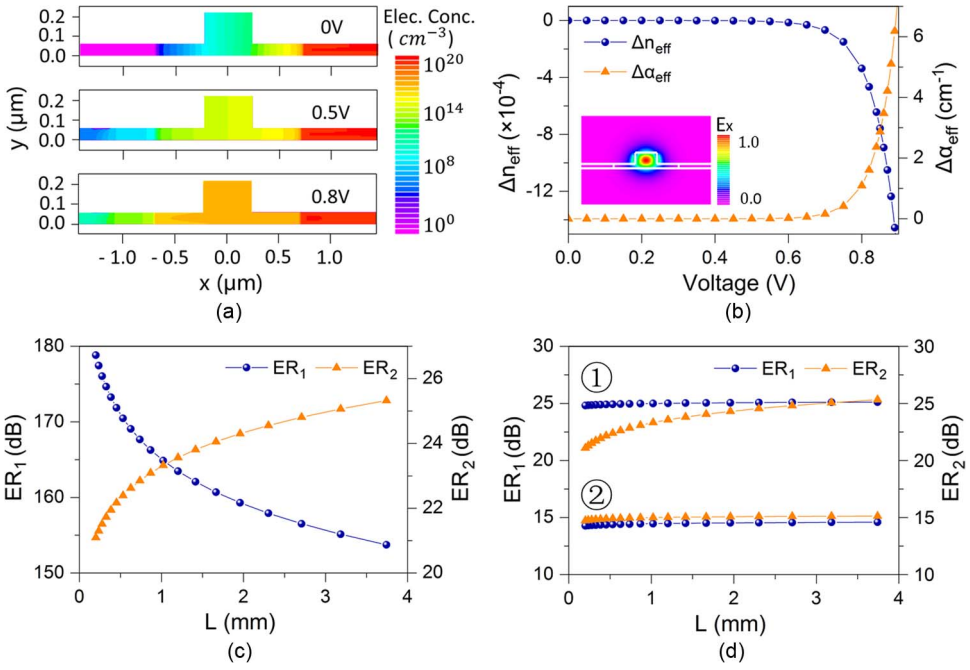

Fig. 3. (a) Electron distribution in the p-i-n diode under 0 V, 0.5 V, and 0.8 V. (b) Effective refractive index and absorption coefficient change with the forward-bias voltage. Inset shows the cross-sectional electric field pattern of the waveguide mode. (c) and (d) Extinction ratios of the single-arm-modulated MZI switch versus arm length. In (c), only the free-carrier absorption effect is considered. In (d), uneven splitting ratio of couplers (grouped as ①) and phase errors in the MZI two arms (grouped as ②) are also considered, in addition to the free-carrier absorption effect.

$$ER_2 = 10\log_{10}\left[\frac{1 + e^{-\Delta\alpha_{eff}L} + 2e^{-\Delta\alpha_{eff}L/2}\cos\theta}{1 + e^{-\Delta\alpha^{m}_{eff}L} - 2e^{-\Delta\alpha^{m}_{eff}L/2}\cos\theta}\right] \tag{17}$$

where $\Delta\alpha_{eff}$ and $\Delta\alpha^{m}_{eff}$ are the overall transmission loss coefficient difference (including scattering loss, bending loss) of the active arm relative to the passive arm under zero and forward-bias, respectively, and θ is the fixed phase difference (phase error) between the MZI arms.

Fig. 3(d) shows the ERs when the uneven splitting ratio or the phase error is considered in addition to the FCA loss. The upper two lines (grouped as ①) are the ERs with a power coupling ratio (κ^2) equal to 0.474 and the lower two lines (grouped as ②) are the ERs with a phase error equal to 20°. Comparing these curves, we can conclude that ER_1 is sensitive to both the power splitting ratio of the couplers and the phase errors in the two arms, and ER_2 is mainly affected by the difference in waveguide propagation loss between passive and active arms (caused by the FCA loss).

2.3. Waveguide Loss

Long length waveguides are needed to achieve a large delay and hence waveguide propagation loss has to be taken into account in designing the feed-forward ODL. The waveguide propagation loss has two effects: firstly, it leads to the attenuation of the delayed optical signal; secondly, since each pair of waveguides have different lengths, the main and residual signals experience different attenuation, which changes the SCR.

The passive waveguide propagation loss includes scattering loss and bending loss. The scattering loss comes from the imperfect fabrication of the waveguide. According to the theory of Payne and Lacey, the surface roughness should be within 1 nm to get < 1.0 dB/cm scattering loss [27]. Waveguide bending, which is necessary to make device compact, causes radiation loss but usually can be suppressed to < 0.1 dB/90° with a proper bending radius.

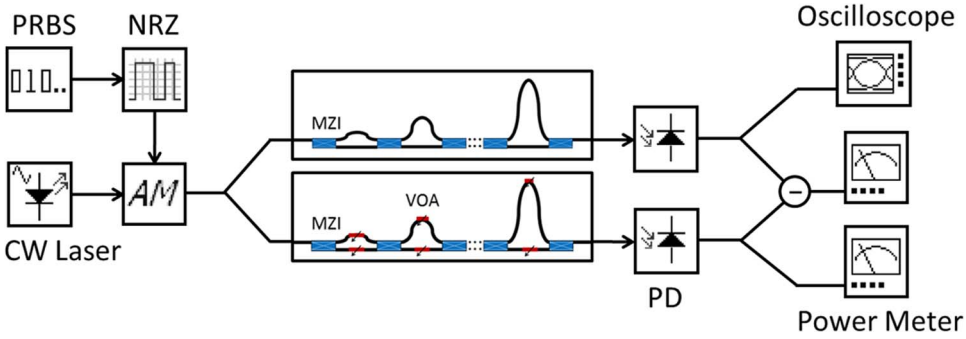

Fig. 4. Simulation setup for crosstalk extraction. CW Laser: continuous wave light source; PRBS: pseudo-random bit sequence generator; NRZ: NRZ electrical pulse generator; AM: amplitude modulator; PD: photodetector.

The submicron silicon-on-insulator (SOI) waveguides fabricated by regular fabrication process have propagation loss of 2.0–3.6 dB/cm [28], [29]. SOI waveguides with less than 1.0 dB/cm loss have also been demonstrated in the literature. Several groups have reported shallow-ridge or thin silicon waveguides with 0.3–1.0 dB/cm loss based on a selective oxidation fabrication technique [30]–[33]. Therefore, it is reasonable to assume 1.0 dB/cm average waveguide propagation loss in our ODL.

3. Simulation Results

We assume the reconfigured feed-forward ODL is composed of 7 stages of waveguide pairs connected by 8 MZI switches. The length difference of the waveguide pair in the kth stage is $2^{k-1} \times 1.765$ mm, and the short waveguide in each stage is 1 mm. The waveguide is estimated to have an average loss of 1.0 dB/cm and a group index of 4.25 [34]. Therefore, the ODL is discretely tunable with a 25 ps delay step. The MZI has an arm length of 0.89 mm with a π-phase shift voltage $V_\pi \cong 0.86$ V. Each MZI is supposed to have a 20° phase error between the two arms and a 0.474 power splitting ratio of the couplers which together lead to an ER ~15 dB as analyzed in Section 2.2. The losses for a single MZI in the "cross" and "bar" states are 0.9 dB and 1.5 dB, respectively including coupling loss, waveguide propagation loss, and FCA loss.

We use a 40 Gbit/s NRZ $2^{13} - 1$ PRBS optical signal at 1550 nm as the input signal to characterize the performance of the proposed ODL. The device can be configured to delay from 8 to 135 bits (1 bit equal to 25 ps) according to Eqs. (6)–(8). The linewidth of the laser light source is assumed to be 10 MHz. The coherence length is calculated to be $L = c/(n_{Si}\Delta f) = 8.77$ m. Since the maximum route length of the ODL is 23.82 cm within the coherence length, it makes sense to calculate the crosstalk based on the interference of different routes. The optical bandwidth of the device is mainly limited by the wavelength dependence of the 3-dB couplers in the MZI switches. However, the switch bandwidth can be up to 100 nm by carefully designing the couplers or using multimode interference (MMI) couplers [22]–[24]. On the other hand, since the optical bandwidth of the 40 Gbit/s NRZ signal is < 1 nm, it is reasonable to assume constant switching ratio across the signal bandwidth.

Fig. 4 is the simulation setup for the ODL. The modulated optical signal is split into two paths and transmitted to two ODLs with VOAs and without VOAs, respectively. The VOAs are assumed to have infinite attenuation so that all the residual signals are get rid of. Hence, the bottom path only contains the pure delayed optical signal with no crosstalk. After they propagate through the ODLs, the optical signals are converted back to the electrical domain by using photodiodes (PD). The signals from the two paths are subtracted to extract the crosstalk. There is no additional system noise in the simulation, so the SCR reflects exactly the influence of the non-ideal MZI switches and waveguide loss on the output signal.

Fig. 5(a) depicts the SCR for every possible delay (8–135 bits) of the device. Overall, the SCR decreases with an increasing delay, because the longer the delay is, the more propagation loss the

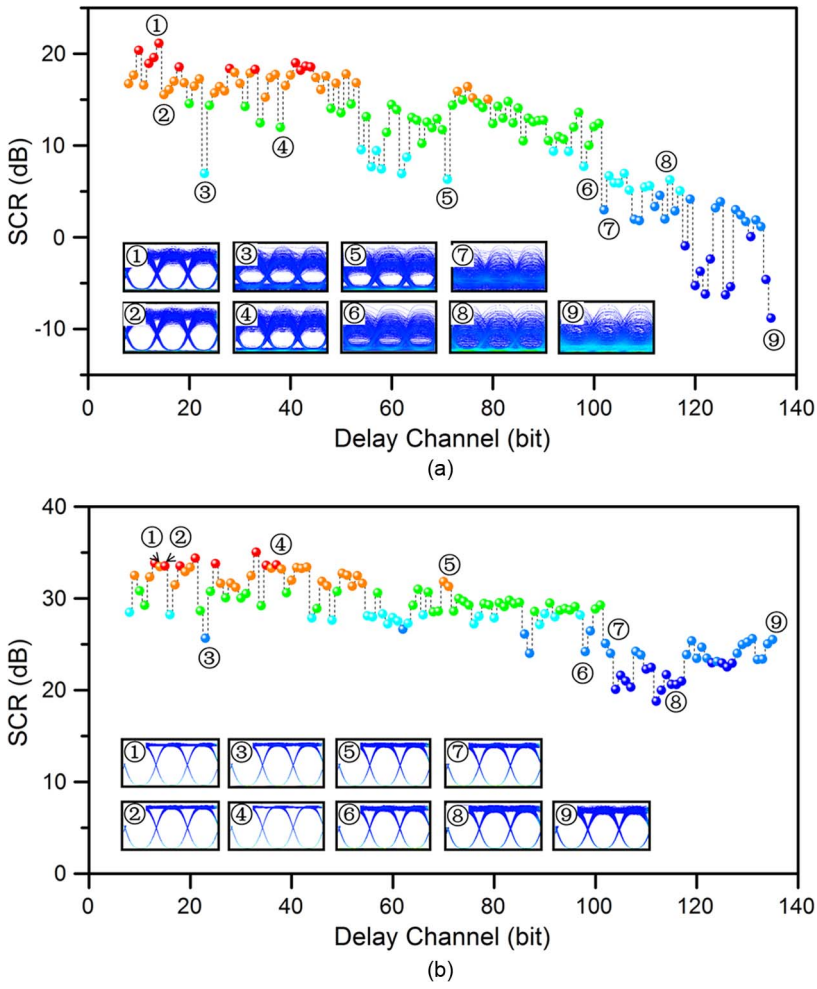

Fig. 5. (a) Simulated SCR of the output signal for each delay channel. Insets show the eye diagrams of the delayed optical signal. (b) Improvement of SCR after using VOAs. Eye diagrams in the insets show the improved signal quality.

signal suffers. Point 1 (delay 14 bits) in Fig. 5(a) has the largest SCR with a clear open eye diagram. Interestingly, the SCR has a sudden drop for certain delays such as points 2–5 (delay 15, 23, 38, and 71 bits, respectively). Those delays are around $(2^{k-1}-1)\Delta t + t_{\min}$, which is most likely due to the constructive interference of the residual signals in the branching routes. For points after 102 bits, a dramatic decrease of SCR occurs. This is because the signal is switched to the two longest waveguides to get more than 104 bits delay $(104 = 2^{7-1} + 2^{6-1} + 8)$ and thus it suffers a significant loss. The small SCR for points 7–9 (102, 115, and 135 bits) indicates the signal is totally submerged in the crosstalk with closed eye diagrams. It is impossible to recover the information from the delayed signal under such delay configurations, which thus implies that the device cannot reach its default maximum capacity. The eye diagram of point 6 (98 bit) is about to close (point 7 has a closed eye diagram), which implies that the buffering capacity of the ODL is 8–98 bits via 91 delay channels.

The simulation result reveals the ODL is limited by the crosstalk and waveguide loss. Accordingly, we can improve the performance of the ODL from two aspects. First approach is to increase the ER of the switch to reduce the crosstalk. Second one is to use low loss waveguide to reduce the signal attenuation. Both of these approaches impose a great challenge to the device design and fabrication.

TABLE 1
Comparison of various integrated optical buffer schemes

	Max delay (ps)	Tuning step (ps)	Loss/Delay (dB/ps)	Power (mW)	Footprint (mm^2)
SCISSOR [10]	345	1.6	0.06	<100	0.027
CROW [11]	800	1	0.01	<500	7
PhCW [13]	103	<1	0.1	<10	0.003
Feed-back ODL [18]	>10,000	1,100	0.002	/	60
Feed-forward ODL (Simulation)	3,375	25	0.007	<320	<10

4. Improvement Using VOAs

We propose to use p-i-n diode based silicon VOAs to eliminate the crosstalk and improve the delay performance. The VOAs are inserted into the waveguides in between each adjacent MZIs as shown in Fig. 1(a). For example, if we add VOAs to the waveguide pair at the first stage, the unwanted residual signal generated by the first MZI can be eliminated. Because of the intrinsic binary structure of the ODL [see Fig. 2(c)], the crosstalk caused by the following branch routes are completely removed. The configuration of the VOA is similar to the phase shifters in MZIs as shown in Fig. 1(c) [35]. The only difference is that it relies on the FCA to attenuate optical signal. VOAs with less than 1 mm length have been reported in the literature [36], which can be fit into the shortest waveguide in our ODL.

Fig. 5(b) shows the simulation result by inserting VOAs in the ODL. Each VOA is supposed to have 10 dB attenuation and the eye diagrams at points 1–9 in Fig. 5(a) are illustrated as comparison. The SCR is increased 17 dB on average. The SCR in long delay routes is 10 dB less than the others but still has a minimum 19 dB. Compared with the eye diagrams in Fig. 5(a), the signal quality is considerably improved by suppression of the crosstalk and the buffering capacity is increased to its full capability, which demonstrates the effectiveness of using VOAs to improve the ODL performance.

5. Discussion

Based on the above analysis and simulation, it is possible to fabricate the feed-forward reconfigurable ODL using standard complementary metal-oxide-semiconductor (CMOS) compatible processes [37]. The waveguides in the ODL can be fabricated using deep ultra-violet (DUV) photolithography and plasma dry etched on a SOI wafer. The lateral p-i-n diode can be formed by boron and phosphorus ion implantation in the slab layer beside the waveguide. Finally, aluminum sputtering and patterning can be done to form metal connection.

For a 1-mm-long MZI switch, a low forward bias (e.g., 1 V) is enough to cause a π-phase shift and change the switch from "cross" to "bar" state, and the power consumption to switch the state is < 5 mW [22]–[24]. For a 1-mm-long VOA, a higher forward bias (e.g., 1.5 V) is needed to generate > 10 dB attenuation. The corresponding power consumption per VOA is typically around 40 mW [36]. Therefore, the total power dissipation of our seven-stage ODL is < 40 mW without VOAs and < 320 mW with the addition of VOAs in the worst case.

In practical design, the long waveguides in our ODL need to bend to fit into a small device area. The spacing between waveguides is limited by the active doping width. With a conservative estimation, the waveguide spacing is 20 μm, and hence, the device footprint is < 10 mm^2.

Table 1 compares our proposed reconfigurable feed-forward ODL with several typical state-of-the-art integrated optical buffers including side-coupled integrated spaced sequence of resonator (SCISSOR), coupled-resonator optical waveguide (CROW), photonic crystal waveguide (PhCW), and feed-back ODL. Note that the maximum delay of the SCISSOR and CROW structures is

measured at 10 Gbit/s, while the other three are measured at 40 Gbit/s. A tradeoff between delay and bandwidth should be taken into consideration for CRS optical buffers, while the key merit of ODL lies in the broadband operation due to its non-resonance structure. Overall, the proposed feed-forward ODL is expected to have a good balance among various aspects of performance.

6. Conclusion

We proposed and theoretically analyzed a silicon reconfigurable feed-forward ODL to achieve step-type tunable optical delay. The ODL is composed of MZI switches and waveguide delay pairs with an incremental length difference. Major factors that degrade the buffered optical signal and restrict the buffering capacity include crosstalk induced by the limited ER of MZI switches and the waveguide loss. We used a 40 Gbit/s NRZ $2^{13} - 1$ PRBS optical signal to analyze the signal quality after ODL. Simulation results reveal that the SCR deteriorates significantly for large delays. Eye diagram shows that the buffering capacity of the ODL is 8–98 bits by using 91 delay channels. To improve the delayed signal quality, we proposed to insert VOAs at each delay stage to eliminate residual signals that causes crosstalk. The SCR is increased 17 dB on average by using VOAs with 10 dB attenuation, and the buffering capacity of the ODL is expanded to 8–135 bits at its maximum.

References

[1] R. S. Tucker, P. C. Ku, and C. J. Chang-Hasnain, "Slow-light optical buffers: Capabilities and fundamental limitations," *J. Lightwave Technol.*, vol. 23, no. 12, pp. 4046–4066, Dec. 2005.

[2] C. J. Chang-Hasnain, K. Pei-Cheng, K. Jungho, and S.-L. Chuang, "Variable optical buffer using slow light in semiconductor nanostructures," *Proc. IEEE*, vol. 91, no. 11, pp. 1884–1897, May 2003.

[3] J. B. Khurgin, "Optical buffers based on slow light in electromagnetically induced transparent media and coupled resonator structures: Comparative analysis," *J. Opt. Soc. Amer. B, Opt. Phys.*, vol. 22, no. 5, pp. 1062–1074, May 2005.

[4] R. W. Boyd, D. J. Gauthier, and A. L. Gaeta, "Applications of slow light in telecommunications," *Opt. Photon. News*, vol. 17, no. 4, pp. 18–23, Apr. 2006.

[5] H. Lee, T. Chen, J. Li, O. Painter, and K. J. Vahala, "Ultra-low-loss optical delay line on a silicon chip," *Nat. Commun.*, vol. 3, no. 5, pp. 1–7, May 2012.

[6] L. Liu, R. Kumar, K. Huybrechts, T. Spuesens, G. Roelkens, E.-J. Geluk, T. de Vries, P. Regreny, D. V. Thourhout, R. Baets, and G. Morthier, "An ultra-small, low-power, all-optical flip-flop memory on a silicon chip," *Nat. Photon.*, vol. 4, no. 3, pp. 182–187, Mar. 2010.

[7] F. Xia, L. Sekaric, and Y. Vlasov, "Ultracompact optical buffers on a silicon chip," *Nat. Photon.*, vol. 1, no. 1, pp. 65–71, Jan. 2007.

[8] Y. A. Vlasov, M. O'Boyle, H. F. Hamann, and S. J. McNab, "Active control of slow light on a chip with photonic crystal waveguides," *Nature*, vol. 438, no. 7064, pp. 65–69, Nov. 2005.

[9] E. F. Burmeister, D. J. Blumenthal, and J. E. Bowers, "A comparison of optical buffering technologies," *Opt. Switching Netw.*, vol. 5, no. 1, pp. 10–18, Jan. 2008.

[10] P. A. Morton, J. Cardenas, J. B. Khurgin, and M. Lipson, "Fast thermal switching of wideband optical delay line with no long-term transient," *IEEE Photon. Technol. Lett.*, vol. 24, no. 6, pp. 512–514, Mar. 2012.

[11] A. Melloni, F. Morichetti, C. Ferrari, and M. Martinelli, "Continuously tunable 1 byte delay in coupled-resonator optical waveguides," *Opt. Lett.*, vol. 33, no. 20, pp. 2389–2391, Oct. 2008.

[12] F. Liu, Q. Li, Z. Zhang, M. Qiu, and Y. Su, "Optically tunable delay line in silicon microring resonator based on thermal nonlinear effect," *IEEE J. Sel. Topics in Quantum Electron.*, vol. 14, no. 3, pp. 706–712, May/Jun. 2008.

[13] J. Adachi, N. Ishikura, H. Sasaki, and T. Baba, "Wide range tuning of slow light pulse in SOI photonic crystal coupled waveguide via folded chirping," *IEEE J. Sel. Topics in Quantum Electron.*, vol. 16, no. 1, pp. 192–199, Jan./Feb. 2010.

[14] L. Juntao, T. P. White, L. O'Faolain, A. Gomez-Iglesias, and T. F. Krauss, "Systematic design of flat band slow light in photonic crystal waveguides," *Opt. Exp.*, vol. 16, no. 9, pp. 6227–6232, Apr. 2008.

[15] S. Kubo, D. Mori, and T. Baba, "Low-group-velocity and low-dispersion slow light in photonic crystal waveguides," *Opt. Lett.*, vol. 32, no. 20, pp. 2981–2983, Oct. 2007.

[16] J. D. LeGrange, J. E. Simsarian, P. Bernasconi, L. Buhl, J. Gripp, and D. T. Neilson, "Demonstration of an integrated buffer for an all-optical packet router," *IEEE Photon. Technol. Lett.*, vol. 21, no. 12, pp. 781–783, Jun. 2009.

[17] E. F. Burmeister, J. P. Mack, H. N. Poulsen, M. L. Masanovic, B. Stamenic, D. J. Blumenthal, and J. E. Bowers, "Photonic integrated circuit optical buffer for packet-switched networks," *Opt. Exp.*, vol. 17, no. 8, pp. 6629–6635, Apr. 2009.

[18] H. Park, J. P. Mack, D. J. Blumenthal, and J. E. Bowers, "An integrated recirculating optical buffer," *Opt. Exp.*, vol. 16, no. 15, pp. 11 124–11 131, Jul. 2008.

[19] S. A. Schulz, L. O'Faolain, D. M. Beggs, T. P. White, A. Melloni, and T. F. Krauss, "Dispersion engineered slow light in photonic crystals: A comparison," *J. Opt.*, vol. 12, no. 10, p. 104 004, Oct. 2010.

[20] A. Melloni, A. Canciamilla, C. Ferrari, F. Morichetti, L. O'Faolain, T. F. Krauss, R. De La Rue, A. Samarelli, and M. Sorel, "Tunable delay lines in silicon photonics: Coupled resonators and photonic crystals, a comparison," *IEEE Photon. J.*, vol. 2, no. 2, pp. 181–194, Apr. 2010.

[21] T. Baba, "Slow light in photonic crystals," *Nat. Photon.*, vol. 2, no. 8, pp. 465–473, Aug. 2008.
[22] S. Akiyama, T. Baba, M. Imai, T. Akagawa, M. Takahashi, N. Hirayama, H. Takahashi, Y. Noguchi, H. Okayama, T. Horikawa, and T. Usuki, "12.5-Gb/s operation with 0.29-V.cm V pi L using silicon Mach–Zehnder modulator based-on forward-biased pin diode," *Opt. Exp.*, vol. 20, no. 3, pp. 2911–2923, Jan. 2012.
[23] P. Dong, S. Liao, H. Liang, R. Shafiiha, D. Feng, G. Li, X. Zheng, A. V Krishnamoorthy, and M. Asghari, "Submilliwatt, ultrafast and broadband electro-optic silicon switches," *Opt. Exp.*, vol. 18, no. 24, pp. 25 225–25 231, Nov. 2010.
[24] J. Van Campenhout, W. M. J. Green, S. Assefa, and Y. A. Vlasov, "Low-power, 2 $\times$ 2 silicon electro-optic switch with 110-nm bandwidth for broadband reconfigurable optical networks," *Opt. Exp.*, vol. 17, no. 26, pp. 24 020–24 029, Dec. 2009.
[25] R. A. Soref and B. R. Bennett, "Electrooptical effects in silicon," *IEEE J. Quantum Electron.*, vol. QE-23, no. 1, pp. 123–129, Jan. 1987.
[26] L. Friedman, R. A. Soref, and J. P. Lorenzo, "Silicon double-injection electro-optic modulator with junction gate control," *J. Appl. Phys.*, vol. 63, no. 6, pp. 1831–1839, Mar. 1988.
[27] F. P. Payne and J. P. R. Lacey, "A theoretical analysis of scattering loss from planar optical waveguides," *Opt. Quantum Electron.*, vol. 26, no. 10, pp. 977–986, Oct. 1994.
[28] Y. A. Vlasov and S. J. McNab, "Losses in single-mode silicon-on-insulator strip waveguides and bends," *Opt. Exp.*, vol. 12, no. 8, pp. 1622–1631, Apr. 2004.
[29] P. Dumon, W. Bogaerts, V. Wiaux, J. Wouters, S. Beckx, J. Van Campenhout, and R. Baes, "Low-loss SOI photonic wires and ring resonators fabricated with deep UV lithography," *IEEE Photon. Technol. Lett.*, vol. 16, no. 5, pp. 1328–1330, May 2004.
[30] P. Dong, W. Qian, S. Liao, H. Liang, C.-C. Kung, N.-N. Feng, R. Shafiiha, J. Fong, D. Feng, A. V. Krishnamoorthy, and M. Asghari, "Low loss shallow-ridge silicon waveguides," *Opt. Exp.*, vol. 18, no. 14, pp. 14 474–14 479, Jul. 2010.
[31] R. Pafchek, R. Tummidi, J. Li, M. A. Webster, E. Chen, and T. L. Koch, "Low-loss silicon-on-insulator shallow-ridge TE and TM waveguides formed using thermal oxidation," *Appl. Opt.*, vol. 48, no. 5, pp. 958–963, Feb. 2009.
[32] J. Cardenas, C. B. Poitras, J. T. Robinson, K. Preston, L. Chen, and M. Lipson, "Low loss etchless silicon photonic waveguides," *Opt. Exp.*, vol. 17, no. 6, pp. 4752–4757, Mar. 2009.
[33] L. K. Rowe, M. Elsey, N. G. Tarr, A. P. Knights, and E. Post, "CMOS-compatible optical rib waveguides defined by local oxidation of silicon," *Electron. Lett.*, vol. 43, no. 7, pp. 392–393, Mar. 2007.
[34] E. Dulkeith, F. N. Xia, L. Schares, W. M. J. Green, and Y. A. Vlasov, "Group index and group velocity dispersion in silicon-on-insulator photonic wires," *Opt. Exp.*, vol. 14, no. 9, pp. 3853–3863, May 2006.
[35] R. R. Whiteman, A. P. Knights, D. George, I. E. Day, A. Vonsovici, A. A. House, G. F. Hopper, and M. Asghari, "Recent progress in the design; Simulation and fabrication of small cross-section silicon-on-insulator VOAs," in *Proc. Photon. Packag. Integr. III*, vol. 4997, R. A. Heyler, D. J. Robbins, and G. E. Jabbour, Eds., 2003, vol. 4997, pp. 146–156.
[36] S. Park, T. Tsuchizawa, T. Watanabe, H. Shinojima, H. Nishi, K. Yamada, Y. Ishikawa, K. Wada, and S. Itabashi, "Monolithic integration and synchronous operation of germanium photodetectors and silicon variable optical attenuators," *Opt. Exp.*, vol. 18, no. 8, pp. 8412–8421, Apr. 2010.
[37] L. Lu, L. Zhou, X. Sun, J. Xie, Z. Zou, H. Zhu, X. Li, and J. Chen, "CMOS-compatible temperature-independent tunable silicon optical lattice filters," *Opt. Exp.*, vol. 21, no. 8, pp. 9447–9456, Apr. 2013.